fire

MDPI

Article

Burn Severity Drivers in Italian Large Wildfires

Francesco Malandra [1], Alessandro Vitali [1,*], Donato Morresi [2], Matteo Garbarino [2], Daniel E. Foster [3], Scott L. Stephens [3] and Carlo Urbinati [1]

[1] Department of Agricultural, Food and Environmental Sciences, Marche Polytechnic University, Via Brecce Bianche 10, 60131 Ancona, Italy
[2] Department of Agricultural, Forest and Food Sciences, University of Turin, Largo Paolo Braccini 2, 10095 Grugliasco, Italy
[3] Department of Environmental Sciences, Policy and Management, University of California, 130 Mulford Hall #3114, Berkeley, CA 94720-3114, USA
* Correspondence: alessandro.vitali@univpm.it; Tel.: +39-071-220-4599

Abstract: The increase of wildfire incidence in highly populated areas significantly enhances the risk for ecosystems and human lives, activities and infrastructures. In central and southern Italy, recent decades' fire records indicate that 2007 and 2017 were extreme years in terms of the number of fires and total burned area. Among them, we selected large fire events and explored their features and drivers of burn severity. We used a standardized extraction procedure to identify large wildfires (>100 ha) from the MODIS burned areas database and Landsat multi-spectral images. We mapped burn severity with the Relative Difference Normalized Burn Ratio index and explored the main drivers of severity using topographic, land-cover and anthropogenic predictors. We selected 113 wildfires for a collective total burned area of over 100,000 ha. Large fires were more frequent in the southern than in the central and northern regions, especially in July and August. The average fire size was about 900 ha and occurred mainly in shrublands (30.4%) and broadleaf forests (19.5%). With a random forest model, we observed that the highest severity occurred in conifer plantations and shrublands, in highly populated areas and at lower elevations. Burn severity models, at the landscape or regional scales, can be very useful tools for pre- and post-fire forest management planning.

Keywords: fire regime; Landsat imagery; RdNBR; land cover; random forest

Citation: Malandra, F.; Vitali, A.; Morresi, D.; Garbarino, M.; Foster, D.E.; Stephens, S.L.; Urbinati, C. Burn Severity Drivers in Italian Large Wildfires. *Fire* **2022**, *5*, 180. https://doi.org/10.3390/fire5060180

Academic Editors: Fangjun Li and Xiaoyang Zhang

Received: 21 September 2022
Accepted: 28 October 2022
Published: 31 October 2022

1. Introduction

Forest fire regimes have changed throughout history in many landscapes worldwide [1], especially in relation to shifts in anthropogenic activities and climate [2]. Humans have played a major role in shaping landscapes and modifying fuel loads and continuity [1]. Woody fuel density increases observed in many developed countries in recent decades are often the result of fire suppression and reforestation actions that have altered fire regimes [3]. Historically, the Mediterranean area hosts some of the largest and most severe wildfires in Europe, making up 90% of the total European burned area [4]. Since at least the Miocene, fire has been an integral component of Mediterranean ecosystems, and there is evidence that rising global temperatures will alter fire regimes [5]. Recent climate changes and land use/land cover changes in the Mediterranean basin are expected to be synchronous drivers of fire-regime shifts [6,7]. Temperature anomalies and summer droughts [8] are critical in explaining fire occurrences but, especially in the Mediterranean basin, land-use/land cover changes are additional drivers of raising wildfire frequency, size and severity [7,9–11]. The increase in wildfire incidence in such highly populated areas introduces a high risk to human lives, activities and infrastructure. Nearly 200 million people live in just five countries: Greece, Italy, France, Spain and Portugal [12], all featuring an extensive wildland-urban interface (WUI), where the risk of fire spread is exceptionally high. In these countries, the rapid industrialization of the 20th century caused relevant

socio-economic changes, such as the extensive decline of traditional agro-silvo-pastoral practices [13], which led to a progressive migration from rural to urban areas. The decline of forest management and the expansion of woody vegetation in marginal lands [14,15], coupled with rising air temperatures [16], have led to increased fuel loads and wildfire risks [5,17].

Variations in temperature, precipitation and relative humidity can shift fire regimes and change fuel flammability. Wildfires can largely depend on other weather variables, such as droughts and wind speed, which have important effects on fire spread rate and propagation direction [18,19]. Burn severity is one of the most critical elements of a fire regime and is commonly defined as the amount of changes induced by a fire and its effects on vegetation and soils [20,21]. Patterns of burn severity depend on numerous factors, which are themselves shifting in response to climate change. Assessing the role of the multiple factors driving burn severity across different ecosystems is challenging, and the relative importance of individual factors often remains unclear [22]. Topography, climate, fire weather, fuel condition and forest management systems are all influential factors affecting burn severity across multiple spatio-temporal scales and ecosystems [23–26]. Whereas biophysical characteristics are often examined in burn severity assessment [20], the role of anthropogenic factors (e.g., population density and infrastructures) remains poorly explored and unclear, unlike their direct effects on forest fire frequency, risk and ignition [27]. This topic can be studied at diverse spatio-temporal scales, ranging from the analysis of single fire events [28] to those at a broader scale with multiple fires [23,25], and with several methods ranging from field data samples to remote sensing analysis.

The use of satellite imagery has significantly improved the monitoring of wildfire occurrence and severity [29]. Advancing technology of optical sensors and related machine learning algorithms has increased the detection of burned areas for improved forest fire prevention and management [30]. Coarse spatial resolution data, such as Moderate Resolution Imaging Spectroradiometer (MODIS) [31] and Visible Infrared Imaging Radiometer Suite (VIIRS) images [32], have been widely used in land-cover/vegetation products [29]. In addition, Sentinel-2 (MSI) and Landsat TM/ETM+/OLI imageries increased the assessment of vegetation response to disturbances at finer scales worldwide [30,33]. Multi-spectral images of burned areas have been analyzed with visual interpretation, supervised classification methods and time series analysis [21,30,34]. Furthermore, several spectral vegetation indices are widely used for efficiently detecting fire-affected areas [35,36]. Burned areas and burn severity can be well detected by combining the red, near-infrared (NIR) and short-wave infrared (SWIR) bands, such as the Normalized Difference Vegetation Index (NDVI) [37], the Enhanced Vegetation Index (EVI) [38] and the Normalized Burn Ratio (NBR) [39]. Bi-temporal indices assessing pre/post-fire conditions, such as the ΔNBR [21], the relativized ΔNBR [40] and the Relativized Burn Ratio (RBR) [41], have been successfully used for burn severity mapping and to quantify ecological changes induced by fires [20,42]. Relativized versions of each spectral index should be preferred since they provide a better assessment of burn severity in heterogeneous landscapes in terms of different vegetation types and a better comparison of spatio-temporal fire-responses of burned areas [40]. A similar more recent index is the Burned Area Index for Sentinel-2 (BAIS2), which exploits the red-edge spectral region [43]. However, the ΔNBR and its relativized version are still largely used in the Mediterranean region [35,36]. Therefore, coupling satellite imagery with standardized field protocols, e.g., the Composite Burn Index protocol proposed by Key and Benson (2006) [21], through statistical and simulation modelling methodologies, has facilitated the production of burn severity maps while minimizing the need for extensive and resource-intensive post-fire field sampling [20].

Forest fires are recurring disturbances in Italy; in the continental area of the Alps, they occur mainly in late winter or spring (especially in the Western sector), but in the more Mediterranean regions of the Apennines and the main islands, they occur mostly in the summer. Within the period 1980–2017, the average annual burned area in Italy was 107,357 ha, and the annual mean number of forest fires was 9121 [44]. Due to changes in fire

policies and prevention, the five-year average burned area in Italy decreased from 147,150 ha in 1980–1989 to 72,945 ha in 2010–2017. Future simulated scenarios predict that Italy, together with other European countries, would experience a significant increase in extreme climatic events [45], likely affecting wildfire frequency and severity. Fire risk forecast and fire control planning are challenging without consistent records and complete time series at the regional or national level [46]. In Italy, the national wildfire inventory is a collection of non-standardized regional records, which is often visually assessed in the field with Global Navigation Satellite System (GNSS) devices after the fire occurrence and lacks the necessary consistency for suitable spatial distribution and severity analysis. A very recent study reports that the most harmonized data are related to the 2004–2012 interval, but these data are not consistent for all the administrative regions nor easily accessible [47].

The landscape simplification, triggered by the overall abandonment of marginal rural areas and forest/shrub expansion that started in the 1950–1960s [13–15], together with climate warming and severe drought events, increased the vulnerability of the Italian peninsula to wildfire ignition, occurrence and severity.

The aims of this work are (i) to map a sample of large-fires in Italy and compute burn severity within their perimeters with Landsat-derived images; (ii) to describe the environmental conditions (geographic distribution, topography and land-cover type) of the selected wildfires; and (iii) to model burn severity using homogenous broad-scale biophysical and anthropogenic predictors. We applied a standardized selection procedure of large forest fires that occurred in peninsular and insular Italy in 2007 and 2017, both years with a high number of fires and large burned areas due to extreme fire weather. We considered "large" a wildfire causing a burned area $\geq$100 hectares, the minimum area used in the literature concerning Mediterranean wildfires (e.g., Mancini et al. 2017 [48]). We hypothesized that pre-fire land cover and anthropogenic factors could be the most influential drivers for fire burn severity in the Mediterranean context. Investigation of burn severity is a crucial aspect for limiting the devastating effects of large forest fires on human lives, infrastructures and environmental resources; and statistical models could be very useful tools for pre- and post-fire forest management planning.

2. Materials and Methods

2.1. The Study Area

The analysis covers 209,198 km^2, 69% of the Italian land surface, extending between 44° and 37° N and 8° to 17° E, from Liguria to Calabria and including the two largest islands (Sicily and Sardinia) (Figure 1). In this area, wildfires occur mainly in the summer months, unlike in the Alpine regions. In the past few decades, socio-economic changes have caused a diffuse abandonment of rural activities and settlements in inland areas and new forests have naturally and extensively expanded in agro-pastoral lands, reducing the landscape heterogeneity and increasing fire risk [13].

Most of the study area is rugged, with 28.7% of the area defined as mountains (areas $\geq$ 600 m a.s.l.) and 50.3% as hills ($\leq$600 m a.s.l.) [49]. The most prominent substrata are terrigenous, clastic and carbonate, with interspersed igneous and metamorphic outcrops. Climatically, the area is characterized by both the temperate (mean annual temperatures of around 10° C and annual precipitation peaks in autumn and spring) and the Mediterranean climate (mean annual temperatures of around 13 °C and summer drought of 2–3 months) [50]. North-eastern slopes (Adriatic side) are, in general, more continental and have higher precipitation than south-western ones (Tyrrhenian side) [15]. Forests, on average, cover over 35% of the national land surface, but in some regions, they surpass 50% (e.g., Liguria, Tuscany, Umbria and Sardinia) [51]. Broadleaf forests occupy approximately 68% of the total forest cover, followed by conifer forests (13.5%) and mixed forests (9.7%) [51]. Fires are more frequent and larger in the southern and insular regions (Sicily, Sardinia, Calabria and Campania), with peaks in July and August [27]. Most forest fires occur in mountain areas and are primarily human-induced (over 75% in 1997–2007) [52]. We extracted a large-wildfire dataset, including two exceptional years, 2007 and 2017, when

a large number of wildfires occurred. In these years, 227,730 ha and 161,987 ha were burned, respectively [44]. The high incidence of wildfire occurrences and total area burned has been driven by the annual climatic anomalies: in 2007, total precipitation was 16% lower and mean temperatures were 1.2 °C higher than average [53]; in 2017, precipitation was 22% lower and temperatures were 1.3 °C higher than average [54].

Figure 1. The study area (green perimeter) includes most of the Italian administrative regions, all featuring summer as the prevailing fire season.

2.2. Wildfire Selection and Burn Severity Assessment

We set up a standardized procedure applied to the entire study area for the fire selection and further processing (Figure 2). We searched for large wildfires (≥100 ha) using MODIS Collection 6 Level 3 (monthly burned area products, MCD64A1, 500 m of spatial resolution) [31]. In QGIS 3.4.0 software, we first filtered the MODIS dataset to keep only burned areas larger than five pixels (about 125 ha). We used the "BurnDate" information derived from the MODIS data product of burned areas to search for Landsat scenes from the United States Geological Survey (USGS) Earth Resources Observation and Science (EROS) Center Science Processing Architecture (ESPA) On-Demand Interface. We collected pre- and post-fire images with the least cloud-contaminated acquisitions (<10% of cloud cover) available during the vegetation growing season. We found 59 Landsat TM and OLI images (30 m spatial resolution) covering the entire study area (Supplementary Materials Table S1).

The latest available pre-fire images before each fire event were used. Then, we used images from the following year to detect the fire scar. Landsat 5 TM-surface reflectance products were generated by the USGS using the Landsat Ecosystem Disturbance Adaptive Processing System (LEDAPS) [55], whereas Landsat 8 OLI image processing was based on the Landsat Surface Reflectance Code (LaSRC) [56]. We masked clouds, cloud shadows and water bodies with the Fmask 3.3 tool in each acquisition [57]. We assessed the fire perimeter and the spatial distribution of burn severity using the Relative Difference Normalized Burn Ratio (RdNBR) [40].

$$\mathrm{NBR} = \frac{\mathrm{NIR} - \mathrm{SWIR2}}{\mathrm{NIR} + \mathrm{SWIR2}} \quad (1)$$

$$dNBR = \left(\left(NBR_{prefire} - NBR_{postfire}\right) \times 1000\right) - dNBR_{offset} \quad (2)$$

$$\mathrm{RdNBR} = \frac{\mathrm{dNBR}}{\sqrt{\left|\mathrm{NBR_{prefire}}\right|}} \quad (3)$$

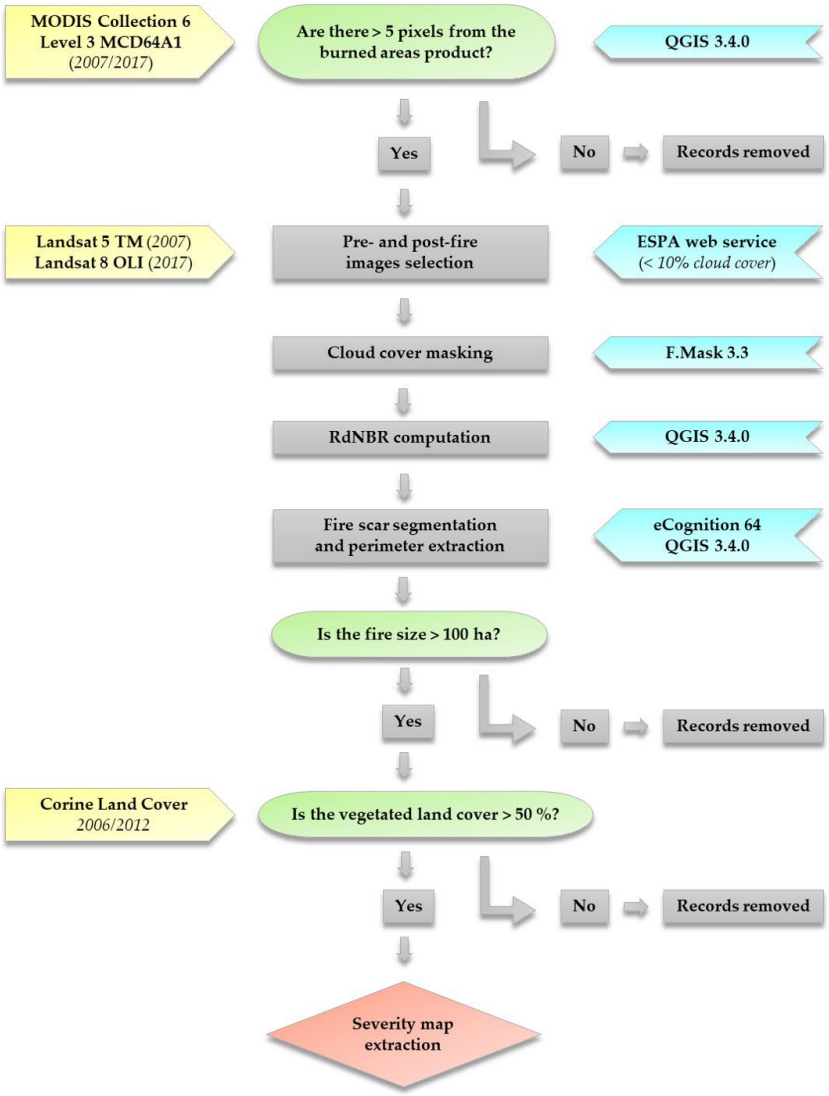

Figure 2. Flowchart of the standardized procedure for wildfire selection, perimeter extraction and burn severity assessment: input data sources (yellow), filtering procedure (green), software used (blue) and output map (pink).

We detected spectral changes one year after the fire as an extended assessment of remotely sensed burn severity, including first- and second-order effects caused by fire [21]. For the severity assessment, we calibrated the dNBR for single wildfires with a dNBR offset; specifically, we averaged dNBR values of pixels falling within two/three undisturbed polygons closest to the fire of the same land-cover types that mainly burned in the event. This procedure minimizes non-fire-induced reflectance variation associated with inter-annual plant phenology and precipitation variability [40,42]. We adopted a semiautomatic method for fire scar segmentation and perimeter extraction. We applied automatic segmentation using eCognition Developer 64 software (scale factor = 30, color factor = 0.5) and a manual on-screen extraction [21] of burned segmented polygons. Then, we corrected perimeters through on-screen digitization of burned pixels in post-fire Landsat TM/OLI

images using false-color composites (RGB = SWIR2, NIR, Red), since misclassification between unchanged and low-severity pixels can frequently occur [36].

Finally, through filtering, we selected the wildfires larger than 100 ha (following Mancini et al. 2017 [48]) and with at least 50% of vegetated land cover types within the perimeters, using CORINE Land Cover (CLC, minimum mapping unit of 25 ha) 2006 (CLC06, [58]) for 2007 and CORINE Land Cover 2012 (CLC12, [59]) for 2017 fires. The filtering retained around 25% of the initial MCD64 burned area records and included 113 selected wildfires that we used in the analysis. For each selected fire, we overlapped the MODIS burned area, the Landsat fire perimeter and the fire severity maps (Figure 3).

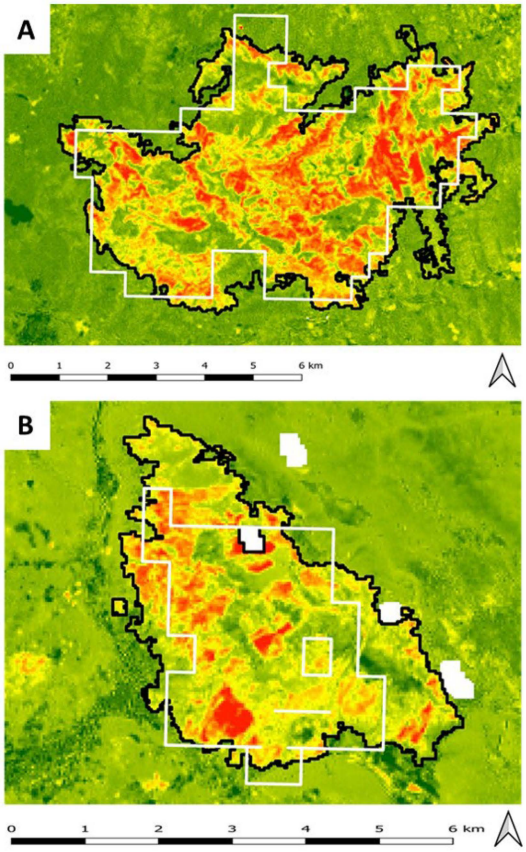

Figure 3. Samples of maps created for all the 113 selected fires. They include the MODIS Collection 6 burned areas (white contour), the fire perimeters (black contour) extracted from Landsat data and the corresponding burn severity maps. Different colors represent the increasing severity, from unburned areas (green) to intermediate (yellow) to high-severity areas (red). White patches are missing values resulting from the cloud masking process. (**A**) Roccafluvione fire (Marche) 2007 (ROC07, 3,110.8 ha); (**B**) Antrodoco fire (Lazio) 2017 (ANT17, 1,149.1 ha). See Table S2 of Supplementary Materials for more information on the selected fires.

2.3. Dataset Creation and Feature Description

We extracted burned surface area (ha), perimeter length (km) and regions of fire occurrence from each fire polygon by working with a homogeneous projected coordinate system (WGS84UTM33N). We attributed each location to the most-represented municipality within each fire perimeter and assigned an identification code (ID) to each event detected (Supplementary Materials Table S2). We used a Digital Elevation Model 20 × 20 m (DEM SINAnet ISPRA) to determine topographic features of the fire surface area: we extracted in the GIS environment elevation (ELE), slope (SLO), Heat Load Index (HLI) as a proxy of slope exposure [60] and Topographic Wetness Index (TWI) as a proxy of terrain wetness [61]. We used CLC06 (2007 fires) and CLC12 (2017 fires) (Level 3-4-5) to check the land-cover types within fire perimeters [62]. We merged the original CLC categories into eleven

larger groups: urban areas (URB), water bodies (WTB), orchards (ORC), croplands (CRP), heterogeneous areas with agriculture and forest (AGF), shrublands (SHB), sparse vegetation (SVG), herbaceous vegetation and grasslands (GRS), broadleaf forests (BRF), conifer forests (COF) and mixed forests (MXF) (Table 1).

Table 1. List of variables used for wildfire feature description and severity model.

Category	Variable Name	Abbreviation	Unit	Source
Topography	Elevation	ELE	m a.s.l.	Derived from DEM SINAnet ISPRA
	Slope	SLO	Degree	
	Heat Load Index	HLI	Adimensional	
	Topographic Wetness Index	TWI	Adimensional	
Land cover	Urban areas	URB	Adimensional	Corine Land Cover 2006/2012
	Water Bodies	WTB		
	Orchards	ORC		
	Croplands	CRP		
	Heterogeneous areas with agriculture and forest	AGF		
	Shrublands	SHB		
	Sparse vegetation areas	SVG		
	Herbaceous vegetation and grasslands	GRS		
	Broadleaf forests	BRF		
	Conifer forests	COF		
	Mixed forests	MXF		
Anthropic	Euclidean distance from state and province roads	ROA	m	National Geoportal database
	Euclidean distance from railroads	RAI	m	OpenStreetMap
	Population density	POP	Inhabitants/km^2	Population census ISTAT 2001/2011

2.4. Severity Modelling

We explored the main drivers of burn severity by modelling within-fire RdNBR using topographic features (ELE, SLO, HLI and TWI) and nine land-cover types (CRP, ORC, AGF, SHB, SVG, GRS, BRF, COF and MXF) as predictors. We excluded urban areas and waterbodies from the analysis. We also included three anthropogenic variables: (i) the Euclidean distance from state and province roads (ROA) extracted from the National Geoportal database [63]; (ii) the Euclidean distance from railroads (RAI) extracted from OpenStreetMap; and (iii) the population density of municipalities that fall within the fire footprint (POP) from the national population census 2001 for 2007 fires and 2011 for 2017 fires [64,65] (Table 1). We used per-pixel RdNBR as the dependent variable, ensuring a comparison of burn severity between different vegetation covers, e.g., shrublands and forests, and pre-fire vegetation densities [40]. We processed all records in a GIS environment, and we spatially joined population densities with their associated municipality vector maps and finally rasterized. We rescaled the spatial resolution of the whole dataset to the Landsat pixel (30 m), and we clipped raster layers with fire perimeters.

We used a large sample of over one million observations from a 30 m point grid where single points correspond to Landsat pixel centroids. We attributed descriptive information (fire ID, fire YEAR), the dependent variable (RdNBR) and predictor values to each point in a GIS environment. Then, we calculated Pearson's correlation matrices of independent quantitative variables to check for multi-collinearity ($R < 0.6$). To limit the influence of spatial autocorrelation, we subsampled observations using a minimum distance of 250 m prior to fitting a Random Forest (RF) regression model [66].The subsampling approach reduced the size of the dataset to 12,961 observations. We checked the degree of intensity

of spatial autocorrelation between the residuals of the RF model at distance steps of 250 m, from 250 to 6000 m, through a semivariogram (Figure S1) computed with the "geoR" R package [67].

The RF model can assess the relationship between Landsat-derived burn severity and several environmental and human-related drivers (Table 1). We employed the RF implementation in the "ranger" [68] R package [69] and optimized hyper-parameters (num.trees = 500; mtry = 1; sample.fraction = 0.2; min.node.size = 10) through the "mlrMBO" R package [70]. To assess the performance of the model, we performed a five-fold spatial cross-validation repeated 10 times and computed the average root mean square error (RMSE). Spatial partitions were based on k-means clustering of observation coordinates and allowed us to maintain independence between training and validation sets [71]. We assessed variable importance through the permutation method [66] and employed partial dependencies [72,73] to interpret the marginal effects of individual predictors on Landsat-derived burn severity.

3. Results

Out of the 113 large wildfires used for the analysis, 49 occurred in 2007 (burned area 56,765 ha) and 64 in 2017 (45,800 ha), for a total burned area of 102,565 ha (Figure 4; Table 2). The mean burned area was 908 ha (±1237) with a range of 108–7474 ha. The largest fire (7474 ha) was recorded in 2007 in Sardinia; the smallest one (108 ha) in Calabria in 2017 (Supplementary Materials Table S2). Most wildfires were in southern Italy (about 75% of fires and 73% of the total burned area), especially in Calabria (n = 34), Sicily (n = 22), Campania (n = 16) and Sardinia (n = 13). Sicily was the most affected region, with a total of 30,769 ha burned in the two years (Table 2).

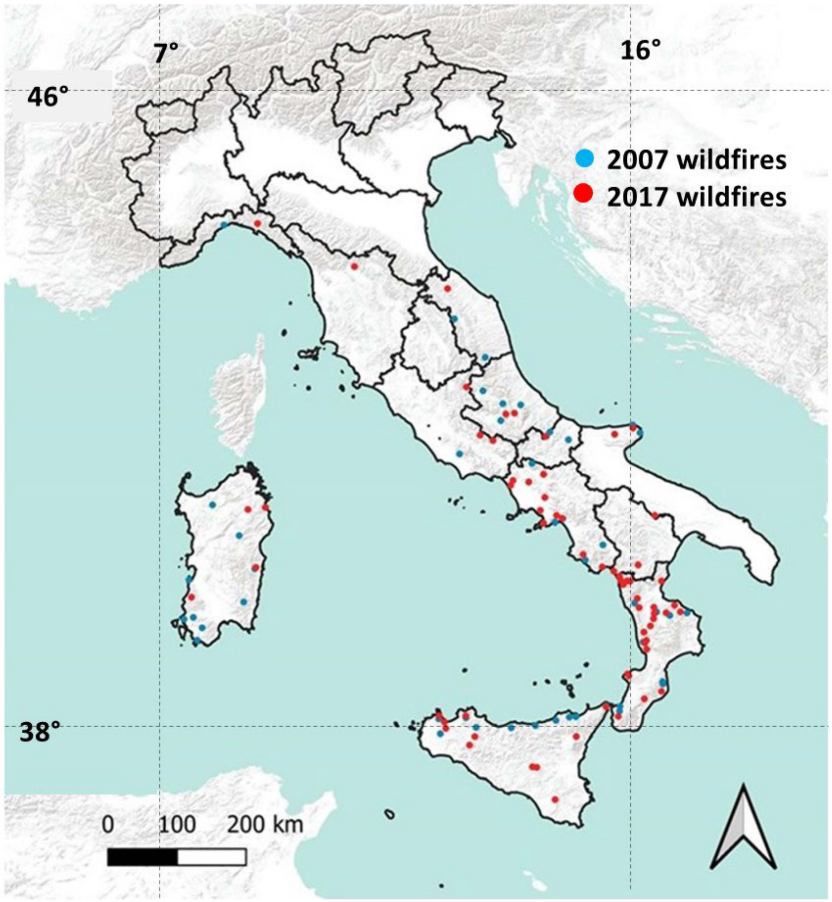

Figure 4. Geographic distribution of the selected large wildfires (>100 ha) with a distinction between 2007 and 2017 fires within the study area.

Table 2. Total number and burned area of large fires in the different regions.

Region	Fires (Count)	Burned Area (ha)
Sicily	22	30,769
Calabria	34	17,619
Sardinia	13	16,452
Abruzzo	9	14,580
Campania	16	9816
Puglia	6	4993
Marche	3	3817
Lazio	4	2071
Liguria	2	1109
Molise	1	507
Basilicata	2	501
Tuscany	1	331
TOTAL	113	102,565

About one-third (36%) of burned areas had an extent ≤500 ha, while those ranging from 250 to 750 ha were about 50% (Figure 5). They mainly occurred in the summer, in July (50%) and in August (42%). These fires occurred within a wide elevation (0–1978 m a.s.l.) and slope (0–76°) range. The main slope aspect varied greatly across the study area. About 43% of the total burned area is in nature conservation areas (e.g., the UE Natura 2000 network and national or regional protected areas).

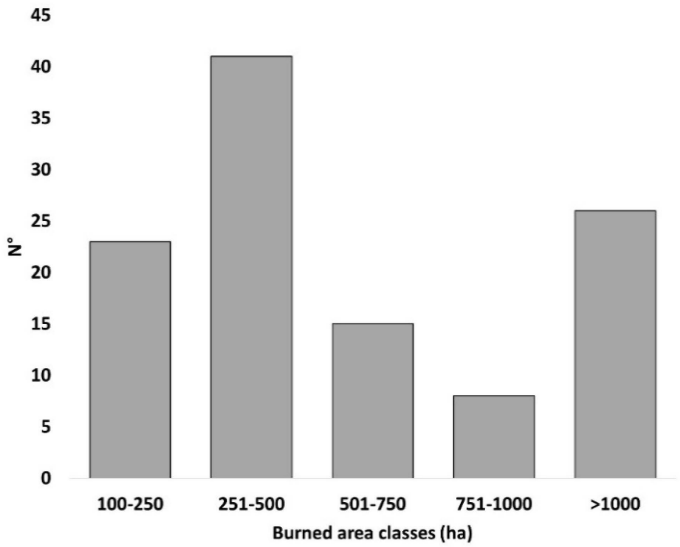

Figure 5. Frequency distribution of fires in burned area classes (ha).

Generally, 30.4% (31,211 ha) of the burned area was shrubland, 19.5% (19,985 ha) was broadleaf forest, 13.1% (13,389 ha) was grassland, 9.4% (9671 ha) was conifer forest and 5.3% (5395 ha) was mixed forests (Table 3).

Conifer forests feature the highest RdNBR mean value in relation to land cover (357, sd = 269), followed by shrubland (293, sd = 245), mixed forests (288, sd = 249) and broadleaf forest (271, sd = 244) (Figure 6).

The RF model highlighted a root-mean-square error of 226.6 and indicated that a distance of 250 m between points effectively reduced spatial autocorrelation as the scaled semivariance at that distance was >0.7.

Table 3. Total area of land cover categories affected by fire within wildfire perimeters. Urban areas and water bodies were excluded. CRP = Cropland, ORC = Orchard, AGF = Heterogeneous areas with agriculture and forest, SHB = Shrubland, SVG = Sparse vegetation area, GRS = Grassland, BRF = Broadleaf forest, COF = Conifer forest, MXF = Mixed forest.

Land Cover Categories	Total Burned Area	
	ha	%
CRP	6220	6.1
ORC	1148	1.1
AGF	13,422	13.1
SHB	31,211	30.4
SVG	1443	1.4
GRS	13,389	13.1
BRF	19,985	19.5
COF	9671	9.4
MXF	5395	5.3

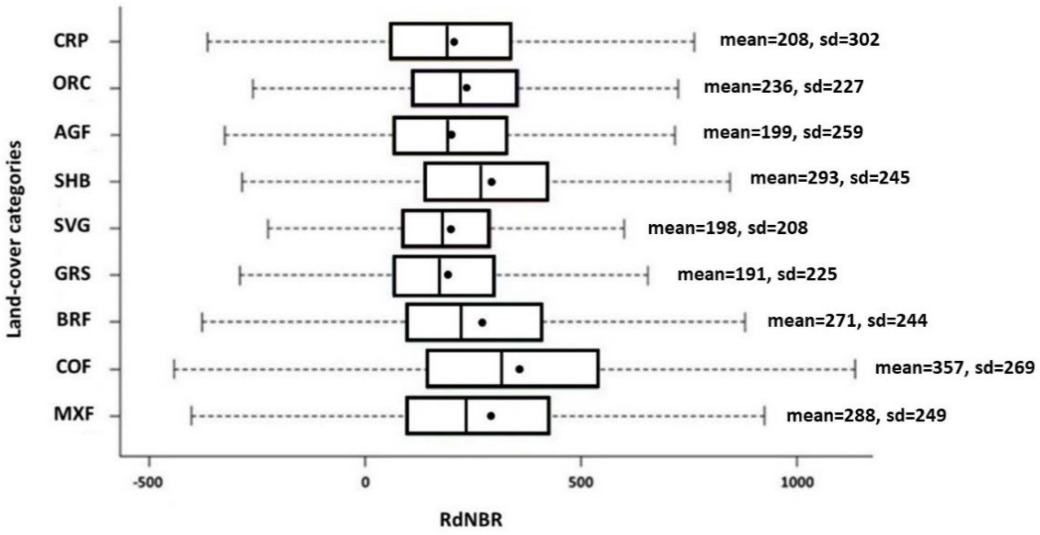

Figure 6. RdNBR values for land-cover categories. Vertical bold lines in the box are the medians. Black dots are the means. Whiskers are the minimum and maximum values. RdNBR mean and standard deviation are shown. CRP = Cropland, ORC = Orchard, AGF = Heterogeneous areas with agriculture and forest, SHB = Shrubland, SVG = Sparse vegetation area, GRS = Grassland, BRF = Broadleaf forest, COF = Conifer forest, MXF = Mixed forest.

The best predictor in the RF model was the pre-fire land cover (CLC; Figure 7). Among land cover categories, RF model output confirmed that conifer forests are largely and positively associated with burn severity, followed, respectively, by shrubland and mixed forests (Figure 8). Higher rates of burn severity were detected at lower elevations, the second most important driver of burn severity (Figure 7) (especially from 0 to approximately 650 m a.s.l.). The models showed a positive relationship between burn severity and population density. We observed high levels of RdNBR in burned areas with more than 3000 inhabitants/km^2. In addition, distance to railroads and roads showed a positive relationship with burn severity (Figures 8 and S2). Slope also showed a positive but weaker relationship with severity, especially increasing between 0 and 16° (Figure S2).

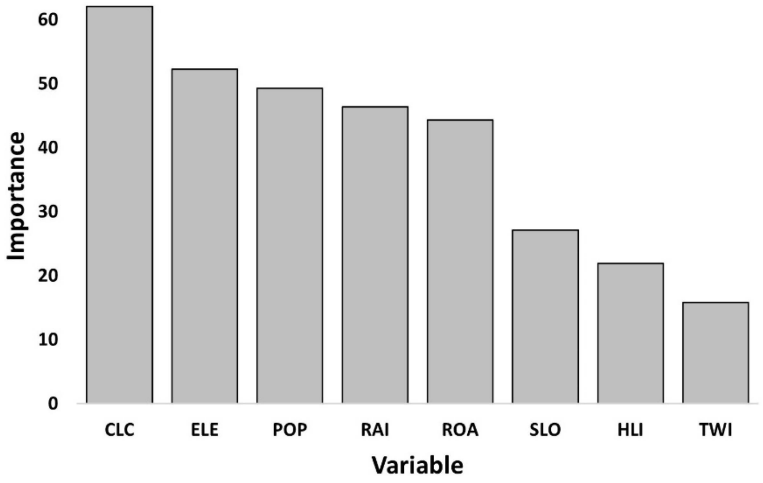

Figure 7. Importance rate of variables in random forest (RF) models of combined fires (grey). Variables are: CLC = Corine Land Cover, including nine land cover categories; ELE = Elevation; POP = population density; RAI = distance to railroads; ROA = distance to roads; SLO = Slope; HLI = Heat Load Index; TWI = Topographic Wetness Index.

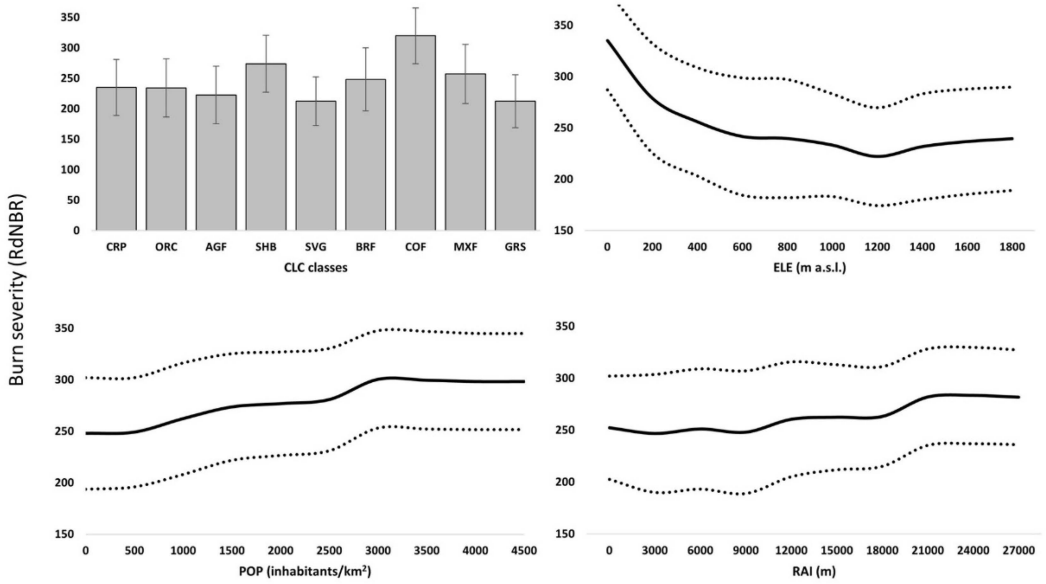

Figure 8. Partial dependence plots showing the relative influences of the four predictors with the highest important rate of burn severity across the respective input data ranges. Solid lines indicate the average over individual marginal effects of each selected explanatory variable (CLC = Corine Land Cover, including nine land cover categories; ELE = elevation; POP = population density; RAI = distance to railroads), whereas dotted lines are the standard deviations of individual marginal effects (+/− 1SD). A bar graph with lines (standard deviations) is used for categorical predictors (CLC).

4. Discussion

Since many ecosystems worldwide are experiencing fire regime shifts in response to changes in climate, land use and land cover [3,5,74,75], investigations into the increasing frequency, size and severity of wildfires are becoming necessary for adopting appropriate management practices. In this work, we analyzed two target years (2007 and 2017), providing a large fire sample size for our investigation. The mean size of all the Italian fires is much lower compared to that of the fires selected, probably due to the increasing effort committed to fire suppression [76]. We considered only large wildfires since their occurrence, expansion and severity are more likely to be influenced by climatic conditions [11].

Moreover, they are expected to increase in the future given climate and land use change trends [11]. A large accumulation of fuels and the increasing fire intensity can easily drive wildfires out of control [11].

Most of the 113 fires occurred in July and August [44,51,77]. Large fires were more numerous in southern Italy, suggesting the importance of other factors such as differences in land ownership forms, regional law and regulations, and efficiency in forest prevention and fire suppression systems. In addition, recently, a relevant administrative change occurred in Italy. Until 2016, the national wildfire control system was coordinated by the National Forest Service (NFS) through their regional headquarters in synergy with the regional offices of the National Civil Protection (NCP) and their local firefighting corps. Thereafter, a newly enforced law limited the tasks of the NFS only to post-fire investigations and transferred all the fire extinction and prevention functions and the related equipment (land and air vehicles) to the NCP [27,51]. These indirect factors might have acted as noise when detecting direct relationships between spatial covariates, fire occurrence and severity.

The results of the analysis on land-cover types affected by large fires in the two target years showed that a large share of the total burned area (65%) was covered by shrubland and forests (mostly broadleaf). The co-occurrence of shrub and forest cover is a common trait of the landscape mosaics in many Mediterranean ecosystems. This is the effect of widespread secondary succession in abandoned agro-pastoral lands [15,78]. Shrubland is a very heterogeneous land-cover category in terms of species composition, structure and fuel characteristics and, together with conifer forest, is very prone to burning in the Mediterranean biome, particularly in southern Spain, France, Italy and Greece [79,80]. Generally, the shrub-forest systems burned extensively, up to 65% of the total burned area. The CLC is broadly used to assess land cover in burned areas [48,81]; however, the 25 ha of minimum mapping unit, used to describe vegetation type, could affect the precision of these estimates. Its spatial resolution and classification structure were conceived to fit a broad range of environmental EU regions and not individual countries [62].

Applied technologies and analytical methods for fire mapping and severity assessment have greatly improved in recent years [30,42,43,82]. Common indices (e.g., dNBR and RdNBR) are still broadly used in fire science [28,35,42], even though precautions in imagery selection are necessary to minimize the differences in phenology, solar angle and sensor calibration. In addition to single-image selection, composite techniques that use imagery over the entire fire season might be another robust way to compute common spectral vegetation indices [83]. In our case, combining a coarse resolution dataset (MODIS Collection 6) [34] with Landsat single-scene data made possible the detection and extraction of numerous fire records. Moreover, Landsat data guaranteed the coverage of a broad geographic area and the same spatial resolution for all the severity maps computed. We used RdNBR, a suitable spectral vegetation index for mapping fire perimeter and assessing burn severity across multiple wildfires featuring a wide range of topographic features, land cover and fire history [24]. The use of a suitable index and a spatially coherent and comprehensive large-scale dataset are basic ingredients to suitably assess the environmental response to fires at the regional scale. However, RdNBR values can be influenced and biased by several factors, such as short-term vegetation recovery of non-forest land covers, fire suppression (land and airborne) and post-fire (e.g., salvage logging) management actions. Nonetheless, severity assessment is strictly related to the method applied: we used spectral changes caused by fire during the vegetative season following the event, defined as an extended assessment of remotely sensed burn severity [21]. This method accounts for first- and second-order effects caused by fire and includes delayed survivorship and mortality of vegetation [84]. Such an approach is widely used for forest and sometimes shrubland fires [85], but it can underestimate the burn severity of some land-cover types (e.g., grasslands) since a limited amount of regrowth of grasses/shrubs is common in the following vegetative season [84]. In addition, a systematic measure of burn severity in the field in many areas, despite the efforts needed, could be useful to better relate these common indices to on-the-ground fire effects [39].

Our modelling approach included land cover, anthropogenic variables and topography as possible drivers of burn severity. Its assessment in human-shaped landscapes is a very complex task because of the heterogeneity of structure and environmental constraints of landscape mosaics and of the poorly explored role of anthropogenic factors (e.g., population density and infrastructures). Our model showed that land cover was the most influential variable affecting burn severity. Several studies have highlighted the relevance of land cover, pre-fire vegetation types and greenness on burn severity in Canadian and Mediterranean forests [86,87]. Even if a metric of pre-fire vegetation cover/greenness such as NDVI can be a suitable predictor of burn severity, we used discrete data showing pre-fire types of land cover. The highest mean severity was found in conifer forests (RdNBR = 357), followed by shrublands (RdNBR = 293) and mixed forests (RdNBR = 288). It is well known that vegetation type is one of the main factors controlling burn severity computed with remotely sensed NB [40]. Conifer forests are more flammable than broadleaf forests due to their higher content of resins, terpenes and their lower foliage moisture content [88], leading to possible higher rates of burn severity, as detected by other studies in Mediterranean ecosystems [89]. Extended shrub cover can foster fire spread and burn with high severity.

Together with the amount and composition of live vegetation and dead fuel [28], topography, which directly influences fire behavior [19], can affect severity as found in several ecosystem types, as reported in the western US, China and Spain [23–25,90]. Our results indicate that elevation was the second most influential predictor in the model, suggesting that burn severity increased at lower elevations and secondarily on the steepest sites. Climate conditions could enhance fire ignition and spread in lower elevation areas, directly affecting burn severity. Although the topographic wetness index and the heat load index are the least important variables in the model, burn severity slightly decreased with the increasing rate of soil moisture. HLI showed no significant trend, although more exposed slopes where solar radiation is higher can affect soil moisture, fuel composition and density [91]. In Mediterranean areas, anthropogenic factors can increase forest fire risk, ignition and frequency [27,92], but their direct effects on burn severity remain unclear. Our findings suggest that population density was the third most important variable in the model, indicating a higher rate of burn severity in highly populated areas. Distance to railroads and, secondarily, distance to roads also showed a positive relationship with burn severity. A denser population could enhance the probability of ignition and frequency of wildfires [92]. Even if a higher rate of ignitions in populated areas can increase fire occurrence, if suppression systems are efficient, they could more likely reduce fire spread and burn severity. Out-of-control fires tend to be more severe in more prone-to-burn landscapes and forest types, such as conifer plantations, generally located at lower elevations, with warmer climatic conditions and where population density tends to be higher. Population density generally decreases at higher elevations where forest ecosystems and landscapes are less prone to burning and climatic conditions could reduce burn severity. Moreover, road network accessibility was found to be spatially related to human-induced fire ignitions in the US, Spain and Italy [92–96]. Infrastructure may affect not only fire ignitions but also their expansion and severity since fire suppression systems are largely dependent on road networks. Areas farther from infrastructure might be more affected by uncontrolled wildfires, leading to higher burn severities.

Fire expansion and severity can be reduced with specific vegetation management actions. It is well known that selective thinning and other specific silvicultural treatments can lower horizontal and vertical fuel continuity by decreasing living and dead fuel loads and modifying forest structure towards a more open canopy cover [86]. In combination with managed wildfires and prescribed fires, these actions can reduce tree density and fuel load at a landscape scale [97], mitigating the fire severity [98,99]. Such aspects, despite not directly investigated by our research, are crucial and should be evaluated for fire severity mitigation strategies.

5. Conclusions

Large wildfires in Mediterranean countries can cause severe environmental and socio-economic impacts, but the analysis of their occurrence, dynamics and severity can provide relevant information for monitoring and implementing control strategies. The availability of complete and consistent records (i.e., burned area) on a national or sub-national scale is essential for understanding wildfire behavior, identifying the most influential fire drivers and implementing appropriate control strategies. The widespread forest expansion and the resultant landscape simplification triggered by the 1950–1960s overall abandonment of marginal rural areas [15] have increased the vulnerability of these areas to wildfire. Predicted climate warming and drought worsening in the Mediterranean basin, together with the increasing share of unmanaged forests and rangelands in marginal areas, can considerably raise the risk of fire ignition and consequent severity [100]. We mapped large wildfires that occurred in peninsular and insular Italy in two target years (2007 and 2017) and modelled burn severity using environmental, topographic and anthropic predictors. The selected 113 large fires have been more frequent in the southern region than in the central and northern regions. The average fire size was about 900 ha (±1240 ha) and occurred mainly in shrublands (30.4%) and broadleaf forests (19.5%). The highest severity occurred in conifer plantations and shrublands, in highly populated areas and at lower elevations. Burn severity models, at least at the landscape or regional scales, are very useful tools for pre- and post-fire forest management planning. Monitoring wildfire hazards and fire impacts on forest ecosystems is also necessary for efficient management of fire prevention and control. The final goal is to reduce the devastating effects of large forest fires on human lives, infrastructures and environmental resources. This is especially true in Mediterranean countries, where the expansion of wildland–urban interfaces (WUIs) [101] and the related increasing likelihood of dangerous fire events within their boundaries is raising concern among policymakers, land managers and the scientific community for their direct ecological and socio-ecological implications.

Supplementary Materials: The following supporting information can be downloaded at: https://www.mdpi.com/article/10.3390/fire5060180/s1, Table S1: List of Landsat records used in the analysis; Table S2: List of locations and main features of wildfires selected for the analysis; Figure S1: Semivariogram of the random forest model residuals; Figure S2: Partial dependence plots showing relative influences of the four predictors with lower important rate of burn severity across the respective input data ranges.

Author Contributions: Conceptualization, F.M. and C.U.; methodology, F.M. and D.M.; formal analysis, F.M., A.V., D.M. and D.E.F.; data curation, F.M.; writing—original draft preparation, F.M.; writing—review and editing, A.V., D.M., M.G., D.E.F., S.L.S. and C.U.; supervision, C.U. All authors have read and agreed to the published version of the manuscript.

Funding: This research received no external funding.

Institutional Review Board Statement: Not applicable.

Data Availability Statement: Not applicable.

Acknowledgments: We wish to thank Enrico Tonelli for his contribution to data analysis and interpretation.

Conflicts of Interest: The authors declare no conflict of interest.

References

1. Pausas, J.G.; Keeley, J.E. A Burning Story: The Role of Fire in the History of Life. *Bioscience* **2009**, *59*, 593–601. [CrossRef]
2. Marlon, J.R.; Bartlein, P.J.; Carcaillet, C.; Gavin, D.G.; Harrison, S.P.; Higuera, P.E.; Joos, F.; Power, M.J.; Prentice, I.C. Climate and human influences on global biomass burning over the past two millennia. *Nat. Geosci.* **2008**, *1*, 697–702. [CrossRef]
3. Stephens, S.L.; Agee, J.K.; Fulé, P.Z.; North, M.P.; Romme, W.H.; Swetnam, T.W.; Turner, M.G. Managing forests and fire in changing climates. *Science* **2013**, *342*, 41–42. [CrossRef] [PubMed]
4. Camia, A.; Amatulli, G. Weather Factors and Fire Danger in the Mediterranean. In *Earth Observation ofWildland Fires in Mediterranean Ecosystems*; Chuvieco, E., Ed.; Springer: Berlin/Heidelberg, Germany, 2009; pp. 71–82. ISBN 9783642017537.

5. Pausas, J.G.; Fernández-Muñoz, S. Fire regime changes in the Western Mediterranean Basin: From fuel-limited to drought-driven fire regime. *Clim. Change* **2012**, *110*, 215–226. [CrossRef]
6. Bajocco, S.; Pezzatti, G.B.; Mazzoleni, S.; Ricotta, C.; Boris, G.; Mazzoleni, S.; Ricotta, C. Wildfire seasonality and land use: When do wildfires prefer to burn? *Environ. Monit. Assess.* **2010**, *164*, 445–452. [CrossRef]
7. Mantero, G.; Morresi, D.; Marzano, R.; Motta, R.; Mladenoff, D.J.; Garbarino, M. The influence of land abandonment on forest disturbance regimes: A global review. *Landsc. Ecol.* **2020**, *35*, 2723–2744. [CrossRef]
8. Dimitrakopoulos, A.P.; Vlahou, M.; Anagnostopoulou, C.G.; Mitsopoulos, I.D. Impact of drought on wildland fires in Greece: Implications of climatic change? *Clim. Change* **2011**, *109*, 331–347. [CrossRef]
9. Dupire, S.; Curt, T.; Bigot, S.; Fréjaville, T. Vulnerability of forest ecosystems to fire in the French Alps. *Eur. J. For. Res.* **2019**, *138*, 813–830. [CrossRef]
10. García-Llamas, P.; Suárez-Seoane, S.; Fernández-Manso, A.; Quintano, C.; Calvo, L. Evaluation of fire severity in fire prone-ecosystems of Spain under two different environmental conditions. *J. Environ. Manage.* **2020**, *271*, 110706. [CrossRef]
11. San-Miguel-Ayanz, J.; Moreno, J.M.; Camia, A. Analysis of large fires in European Mediterranean landscapes: Lessons learned and perspectives. *For. Ecol. Manage.* **2013**, *294*, 11–22. [CrossRef]
12. Eatock, D. Demographic Outlook for the European Union 2019. EPRS European Parliamentary Research Service. 2019. Available online: https://www.europarl.europa.eu/thinktank/en/document.html?reference=EPRS_IDA(2019)637955#:~{}:text=The%20EU%20has%20seen%20its,the%20middle%20of%20the%20century (accessed on 1 September 2022). [CrossRef]
13. Malandra, F.; Vitali, A.; Urbinati, C.; Garbarino, M. 70 Years of Land Use/Land Cover Changes in the Apennines (Italy): A Meta-Analysis. *Forests* **2018**, *9*, 551. [CrossRef]
14. Garbarino, M.; Morresi, D.; Urbinati, C.; Malandra, F.; Motta, R.; Sibona, E.M.; Vitali, A.; Weisberg, P.J. Contrasting land use legacy effects on forest landscape dynamics in the Italian Alps and the Apennines. *Landsc. Ecol.* **2020**, *35*, 2679–2694. [CrossRef]
15. Malandra, F.; Vitali, A.; Urbinati, C.; Weisberg, P.J.; Garbarino, M. Patterns and drivers of forest landscape change in the Apennines. *Reg. Environ. Chang.* **2019**, *19*, 1973–1985. [CrossRef]
16. de Rigo, D.; Libertà, G.; Houston Durrant, T.; Artès Vivancos, T.; San-Miguel-Ayanz, J. *Forest Fire Danger Extremes in Europe under Climate Change: Variability and Uncertainty*; EUR 28926 EN; Publications Office of the European Union: Luxembourg, 2017; ISBN 978-92-79-77046-3. Available online: https://ec.europa.eu/jrc/en/publication/forest-fire-danger-extremes-europe-under-climate-change-variability-and-uncertainty (accessed on 1 September 2020). [CrossRef]
17. Ascoli, D.; Moris, J.V.; Marchetti, M.; Sallustio, L. Land use change towards forests and wooded land correlates with large and frequent wildfires in Italy. *Ann. Silvic. Res.* **2021**, *46*, 177–188. [CrossRef]
18. Flannigan, M.; Stocks, B.; Turetsky, M.; Wotton, M. Impacts of climate change on fire activity and fire management in the circumboreal forest. *Glob. Chang. Biol.* **2009**, *15*, 549–560. [CrossRef]
19. Rothermel, R. *A Mathematical Model for Predicting Fire Spread. Intermountain Forest & Range Experiment Station, Forest Service*; US Department of Agriculture: Washington, DC, USA, 1972; pp. 1–48.
20. Morgan, P.; Keane, R.E.; Dillon, G.K.; Jain, T.B.; Hudak, A.T.; Karau, E.C.; Sikkink, P.G.; Holden, Z.A.; Strand, E.K. Challenges of assessing fire and burn severity using field measures, remote sensing and modelling. *Int. J. Wildl. Fire* **2014**, *23*, 1045–1060. [CrossRef]
21. Key, C.H.; Benson, N.C. Landscape Assessment (LA) Sampling and Analysis Methods. In *FIREMON: Fire Effects Monitoring and Inventory System*; General Technical Report; RMRS-GTR-164-CD; USDA Forest Service: Washington, DC, USA; Rocky Mountain Research Station: Fort Collins, CO, USA, 2006.
22. Parks, S.A.; Holsinger, L.M.; Panunto, M.H.; Jolly, W.M.; Dobrowski, S.Z.; Dillon, G.K. High-severity fire: Evaluating its key drivers and mapping its probability across western US forests. *Environ. Res. Lett.* **2018**, *13*, 044037. [CrossRef]
23. Birch, D.S.; Morgan, P.; Kolden, C.A.; Abatzoglou, J.T.; Dillon, G.K.; Hudak, A.T.; Smith, A.M.S. Vegetation, topography and daily weather influenced burn severity in central Idaho and western Montana forests. *Ecosphere* **2015**, *6*, 1–23. [CrossRef]
24. Dillon, G.K.; Holden, Z.A.; Morgan, P.; Crimmins, M.A.; Heyerdahl, E.K.; Luce, C.H. Both topography and climate affected forest and woodland burn severity in two regions of the western US, 1984 to 2006. *Ecosphere* **2011**, *2*, 130. [CrossRef]
25. Fang, L.; Yang, J.; Zu, J.; Li, G.; Zhang, J. Quantifying influences and relative importance of fire weather, topography, and vegetation on fire size and fire severity in a Chinese boreal forest landscape. *For. Ecol. Manage.* **2015**, *356*, 2–12. [CrossRef]
26. Nolè, A.; Rita, A.; Spatola, M.F.; Borghetti, M. Biogeographic variability in wildfire severity and post-fire vegetation recovery across the European forests via remote sensing-derived spectral metrics. *Sci. Total Environ.* **2022**, *823*, 153807. [CrossRef] [PubMed]
27. Michetti, M.; Pinar, M. Forest Fires Across Italian Regions and Implications for Climate Change: A Panel Data Analysis. *Environ. Resour. Econ.* **2019**, *72*, 207–246. [CrossRef]
28. Harris, L.; Taylor, A.H. Topography, Fuels, and Fire Exclusion Drive Fire Severity of the Rim Fire in an Old-Growth Mixed-Conifer Forest, Yosemite National Park, USA. *Ecosystems* **2015**, *18*, 1192–1208. [CrossRef]
29. Kganyago, M.; Shikwambana, L. Assessment of the characteristics of recent major wildfires in the USA, Australia and Brazil in 2018-2019 using multi-source satellite products. *Remote Sens.* **2020**, *12*, 1803. [CrossRef]
30. Filipponi, F. Exploitation of Sentinel-2 Time Series to Map Burned Areas at the National Level: A Case Study on the 2017 Italy Wildfires. *Remote Sens.* **2019**, *11*, 622. [CrossRef]
31. Giglio, L.; Boschetti, L.; Roy, D.P.; Humber, M.L.; Justice, C.O. The Collection 6 MODIS burned area mapping algorithm and product. *Remote Sens. Environ.* **2018**, *217*, 72–85. [CrossRef]

32. Oliva, P.; Schroeder, W. Remote Sensing of Environment Assessment of VIIRS 375 m active fi re detection product for direct burned area mapping. *Remote Sens. Environ.* **2015**, *160*, 144–155. [CrossRef]
33. Roteta, E.; Bastarrika, A.; Padilla, M.; Storm, T.; Chuvieco, E. Development of a Sentinel-2 burned area algorithm: Generation of a small fire database for sub-Saharan Africa. *Remote Sens. Environ.* **2019**, *222*, 1–17. [CrossRef]
34. Boschetti, L.; Roy, D.P.; Justice, C.O.; Humber, M.L. MODIS–Landsat fusion for large area 30 m burned area mapping. *Remote Sens. Environ.* **2015**, *161*, 27–42. [CrossRef]
35. Cardil, A.; Mola-Yudego, B.; Blázquez-Casado, Á.; González-Olabarria, J.R. Fire and burn severity assessment: Calibration of Relative Differenced Normalized Burn Ratio (RdNBR) with field data. *J. Environ. Manag.* **2019**, *235*, 342–349. [CrossRef]
36. Morresi, D.; Vitali, A.; Urbinati, C.; Garbarino, M. Forest Spectral Recovery and Regeneration Dynamics in Stand-Replacing Wildfires of Central Apennines Derived from Landsat Time Series. *Remote Sens.* **2019**, *11*, 308. [CrossRef]
37. Tucker, C.J. Red and Photographic Infrared Linear Combinations for Monitoring Vegetation. *Remote Sens. Environ.* **1979**, *8*, 127–150. [CrossRef]
38. Chen, X.; Vogelmann, J.E.; Rollins, M.; Ohlen, D.; Key, C.H.; Yang, L.; Huang, C.; Shi, H. Detecting post-fire burn severity and vegetation recovery using multitemporal remote sensing spectral indices and field-collected composite burn index data in a ponderosa pine forest. *Int. J. Remote Sens.* **2011**, *32*, 7905–7927. [CrossRef]
39. Benson, N.; Key, C.H. Measuring and remote sensing of burn severity; the CBI and NBR. In Proceedings of the Joint Fire Science Conference and Workshop, Boise, ID, USA, 15–17 June 1999; Volume II.
40. Miller, J.D.; Thode, A.E. Quantifying burn severity in a heterogeneous landscape with a relative version of the delta Normalized Burn Ratio (dNBR). *Remote Sens. Environ.* **2007**, *109*, 66–80. [CrossRef]
41. Parks, S.A.; Dillon, G.K.; Miller, C. A new metric for quantifying burn severity: The relativized burn ratio. *Remote Sens.* **2014**, *6*, 1827–1844. [CrossRef]
42. Morresi, D.; Marzano, R.; Lingua, E.; Motta, R.; Garbarino, M. Mapping burn severity in the western Italian Alps through phenologically coherent reflectance composites derived from Sentinel-2 imagery. *Remote Sens. Environ.* **2022**, *269*, 112800. [CrossRef]
43. Filipponi, F. BAIS2: Burned Area Index for Sentinel-2. *Proceedings* **2018**, *2*, 364. [CrossRef]
44. San-Miguel-Ayanz, J.; Houston Durrant, T.; Boca, R.; Libertà, G.; Branco, A.; de Rigo, D.; Ferrari, D.; Maianti, P.; Vivancos, T.A.; Costa, H.; et al. *Forest Fires in Europe, Middle East and North Africa 2017. EUR 29318 EN* ISBN 978-92-79-92831-4. 2018. Available online: https://ec.europa.eu/jrc/en/publication/forest-fires-europe-milddle-east-and-north-africa-2017 (accessed on 2 September 2020). [CrossRef]
45. Moriondo, M.; Good, P.; Durao, R.; Bindi, M.; Giannakopoulos, C.; Corte-Real, J. Potential impact of climate change on fire risk in the Mediterranean area. *Clim. Res.* **2006**, *31*, 85–95. [CrossRef]
46. Bartolucci, A.; Marconi, M.; Magni, M.; Pierdicca, R.; Malandra, F.; Ho, T.C.; Vitali, A.; Urbinati, C. Combining Participatory Mapping and Geospatial Analysis Techniques to Assess Wildfire Risk in Rural North Vietnam. *Environ. Manage.* **2022**, *69*, 466–479. [CrossRef]
47. Elia, M.; D'Este, M.; Ascoli, D.; Giannico, V.; Spano, G.; Ganga, A.; Colangelo, G.; Lafortezza, R.; Sanesi, G. Estimating the probability of wildfire occurrence in Mediterranean landscapes using Artificial Neural Networks. *Environ. Impact Assess. Rev.* **2020**, *85*, 106474. [CrossRef]
48. Mancini, L.D.; Barbati, A.; Corona, P. Geospatial analysis of woodland fire occurrence and recurrence in Italy. *Ann. Silvic. Res.* **2017**, *41*, 41–47. [CrossRef]
49. ISTAT. Annuario Statistico Italiano (Vol. 1). In Annuario Statistico Italiano, 2005. Available online: https://ebiblio.istat.it/SebinaOpac/resource/annuario-statistico-italiano/IST0010812?tabDoc=taboggd49 (accessed on 1 September 2020)ISSN 00664545.
50. Blasi, C.; Capotorti, G.; Copiz, R.; Guida, D.; Mollo, B.; Smiraglia, D.; Zavattero, L. Classification and mapping of the ecoregions of Italy. *Plant Biosyst.* **2014**, *148*, 1255–1345. [CrossRef]
51. *Rapporto Sullo Stato Delle Foreste e Del Settore Forestale in Italia, RaFITALIA 2017–2018*; 2019; ISBN 9788898850341. Available online: https://www.reterurale.it/flex/cm/pages/ServeBLOB.php/L/IT/IDPagina/19231 (accessed on 1 September 2020).
52. Lovreglio, R.; Leone, V.; Giaquinto, P.; Notarnicola, A. Wildfire cause analysis: Four case-studies in southern Italy. *IForest* **2010**, *3*, 8–15. [CrossRef]
53. Baffo, F.; Desiato, F.; Fioravanti, G.; Frascehtti, P.; Perconti, W.; Toreti, A.; Morucci, S.; Pavan, V.; Cacciamani, C.; Stel, F.; et al. *Gli Indicatori del Clima in Italia nel 2007*; Agenzia per la Protezione Dell'ambiente e per i Servizi Tecnici: Roma, Italy, 2007.
54. Desiato, F.; Fioravanti, G.; Fraschetti, P.; Perconti, W.; Piervitali, E.; Pavan, V. *Gli indicatori del Clima in Italia 2017*; ISPRA—Istituto Superiore per la Protezione e la Ricerca Ambientale: Roma, Italy, 2018; ISBN 978-88-448-0904-1.
55. Masek, J.G.; Vermote, E.F.; Saleous, N.E.; Wolfe, R.; Hall, F.G.; Huemmrich, K.F.; Gao, F.; Kutler, J.; Lim, T.K. A landsat surface reflectance dataset for North America, 1990-2000. *IEEE Geosci. Remote Sens. Lett.* **2006**, *3*, 68–72. [CrossRef]
56. Vermote, E.; Justice, C.; Claverie, M.; Franch, B. Preliminary analysis of the performance of the Landsat 8/OLI land surface reflectance product. *Remote Sens. Environ.* **2016**, *185*, 46–56. [CrossRef]
57. Zhu, Z.; Wang, S.; Woodcock, C.E. Improvement and expansion of the Fmask algorithm: Cloud, cloud shadow, and snow detection for Landsats 4-7, 8, and Sentinel 2 images. *Remote Sens. Environ.* **2015**, *159*, 269–277. [CrossRef]
58. European Environment Agency (EEA). CLC2006 Technical Guidelines. EEA TECHNICAL Report No 17. 2007. Available online: https://www.eea.europa.eu/publications/technical_report_2007_17 (accessed on 1 September 2020).

59. European Environment Agency (EEA). CLC2012 Addendum to CLC2006. Technical Guidelines. 2014. Available online: https://land.copernicus.eu/user-corner/technical-library/Addendum_finaldraft_v2_August_2014.pdf59 (accessed on 1 September 2020).
60. McCune, B.; Keon, D. Equations for potential annual direct incident radiation and heat load. *J. Veg. Sci.* **2002**, *13*, 603–606. [CrossRef]
61. Sørensen, R.; Zinko, U.; Seibert, J. On the calculation of the topographic wetness index: Evaluation of different methods based on field observations. *Hydrol. Earth Syst. Sci.* **2006**, *10*, 101–112. [CrossRef]
62. Land.copernicus.eu. Available online: https://land.copernicus.eu/pan-european/corine-land-cover (accessed on 1 October 2020).
63. PCN.miniambiente.it. Available online: http://www.pcn.minambiente.it/mattm/ (accessed on 1 October 2020).
64. ISTAT. *14° Censimento Generale della Popolazione e delle Abitazioni*; 2001; ISBN IST0047379. Available online: https://www.istat.it/it/censimenti-permanenti/censimenti-precedenti/popolazione-e-abitazioni/popolazione-2001#:~{}:text=Popolazione%202001-,14%C2%B0%20Censimento%20della%20popolazione%20e%20delle%20abitazioni%202001,e%2027%20milioni%20di%20abitazioni (accessed on 1 September 2020).
65. ISTAT. 15° Censimento Generale Della Popolazione e Delle Abitazioni. 2011. Available online: https://www.istat.it/it/censimenti-permanenti/censimenti-precedenti/popolazione-e-abitazioni/popolazione-2011 (accessed on 1 September 2020).
66. Breiman, L. Random Forests. *Mach. Learn.* **2001**, *45*, 5–32. [CrossRef]
67. Diggle, P.J.; Tawn, J.A. Model-based geostatistics. *J. R. Stat. Soc. Ser. C Appl. Stat.* **1998**, *47*, 299–350. [CrossRef]
68. Wright, M.N.; Ziegler, A. Ranger: A fast implementation of random forests for high dimensional data in C++ and R. *J. Stat. Softw.* **2017**, *77*, 1–17. [CrossRef]
69. R Core Team. *R: A Language and Environment for Statistical Computing*; R Foundation for Statistical Computing: Vienna, Austria, 2021; Available online: https://www.r-project.org/ (accessed on 1 September 2022).
70. Bischl, B.; Richter, J.; Bossek, J.; Horn, D.; Thomas, J.; Lang, M. mlrMBO: A Modular Framework for Model-Based Optimization of Expensive Black-Box Functions. *arXiv* **2017**, arXiv:1703.03373.
71. Schratz, P.; Muenchow, J.; Iturritxa, E.; Richter, J.; Brenning, A. Hyperparameter tuning and performance assessment of statistical and machine-learning algorithms using spatial data. *Ecol. Modell.* **2019**, *406*, 109–120. [CrossRef]
72. Friedman, J.H. Greedy function approximation: A gradient boosting machine. *Ann. Stat.* **2001**, *29*, 1189–1232. [CrossRef]
73. Goldstein, A.; Kapelner, A.; Bleich, J.; Pitkin, E. Peeking Inside the Black Box: Visualizing Statistical Learning With Plots of Individual Conditional Expectation. *J. Comput. Graph. Stat.* **2015**, *24*, 44–65. [CrossRef]
74. Gorbatenko, V.P.; Volkova, M.A.; Nosyreva, O.V.; Zhuravlev, G.G.; Kuzhevskaia, I.V. Influence of Climatic Conditions on Western Siberian Forest Fires. In *Predicting, Monitoring, and Assessing Forest Fire Dangers and Risks*; IGI Global: Hershey, PA, USA, 2019; pp. 269–293. ISBN 9781799818670.
75. Lizundia-Loiola, J.; Pettinari, M.L.; Chuvieco, E. Temporal Anomalies in Burned Area Trends: Satellite Estimations of the Amazonian 2019 Fire Crisis. *Remote Sens.* **2020**, *12*, 151. [CrossRef]
76. Agriregionieuropa.univpm.it. Available online: https://agriregionieuropa.univpm.it/ (accessed on 1 September 2020).
77. Schmuck, G.; San-Miguel-Ayanz, J.; Camia, A.; Kucera, J.; Libertá, G.; Boca, R.; Durrant, T.; Amatulli, G.; Schulte, E.; Bucki, M. *Forest Fires in Europe 2007—JRC Scientific and Technical Reports*; Office for Official Publications of the European Communities: Luxembourg, 2008.
78. Gartzia, M.; Alados, C.L.; Perez-Cabello, F. Assessment of the effects of biophysical and anthropogenic factors on woody plant encroachment in dense and sparse mountain grasslands based on remote sensing data. *Prog. Phys. Geogr.* **2014**, *38*, 201–217. [CrossRef]
79. Barros, A.M.G.; Pereira, J.M.C. Wildfire selectivity for land cover type: Does size matter? *PLoS ONE* **2014**, *9*, e84760. [CrossRef]
80. Moreira, F.; Vaz, P.; Catry, F.; Silva, J.S. Regional variations in wildfire susceptibility of land-cover types in Portugal: Implications for landscape management to minimize fire hazard. *Int. J. Wildl. Fire* **2009**, *18*, 563. [CrossRef]
81. Amos, C.; Petropoulos, G.P.; Ferentinos, K.P. Determining the use of Sentinel-2A MSI for wildfire burning & severity detection. *Int. J. Remote Sens.* **2019**, *40*, 905–930. [CrossRef]
82. Hawbaker, T.J.; Vanderhoof, M.K.; Schmidt, G.L.; Beal, Y.J.; Picotte, J.J.; Takacs, J.D.; Falgout, J.T.; Dwyer, J.L. The Landsat Burned Area algorithm and products for the conterminous United States. *Remote Sens. Environ.* **2020**, *244*, 111801. [CrossRef]
83. Parks, S.A.; Holsinger, L.M.; Voss, M.A.; Loehman, R.A.; Robinson, N.P. Mean composite fire severity metrics computed with google earth engine offer improved accuracy and expanded mapping potential. *Remote Sens.* **2018**, *10*, 879. [CrossRef]
84. Key, C.H. Ecological and Sampling Constraints on Defining Landscape Fire Severity. *Fire Ecol.* **2006**, *2*, 34–59. [CrossRef]
85. Vogelmann, J.E.; Kost, J.R.; Tolk, B.; Howard, S.; Short, K.; Chen, X.; Huang, C.; Pabst, K.; Rollins, M.G. Monitoring landscape change for LANDFIRE using multi-temporal satellite imagery and ancillary data. *IEEE J. Sel. Top. Appl. Earth Obs. Remote Sens.* **2011**, *4*, 252–264. [CrossRef]
86. García-Llamas, P.; Suárez-Seoane, S.; Taboada, A.; Fernández-Manso, A.; Quintano, C.; Fernández-García, V.; Fernández-Guisuraga, J.M.; Marcos, E.; Calvo, L. Environmental drivers of fire severity in extreme fire events that affect Mediterranean pine forest ecosystems. *For. Ecol. Manage.* **2019**, *433*, 24–32. [CrossRef]
87. Whitman, E.; Parisien, M.A.; Thompson, D.K.; Hall, R.J.; Skakun, R.S.; Flannigan, M.D. Variability and drivers of burn severity in the northwestern Canadian boreal forest. *Ecosphere* **2018**, *9*, e02128. [CrossRef]
88. Viana-Soto, A.; Aguado, I.; Martínez, S. Assessment of Post-Fire Vegetation Recovery Using Fire Severity and Geographical Data in the Mediterranean Region (Spain). *Environments* **2017**, *4*, 90. [CrossRef]

89. Fernandes, P.M.; Luz, A.; Loureiro, C. Changes in wildfire severity from maritime pine woodland to contiguous forest types in the mountains of northwestern Portugal. *For. Ecol. Manag.* **2010**, *260*, 883–892. [CrossRef]
90. Viedma, O.; Quesada, J.; Torres, I.; De Santis, A.; Moreno, J.M. Fire Severity in a Large Fire in a Pinus pinaster Forest is Highly Predictable from Burning Conditions, Stand Structure, and Topography. *Ecosystems* **2015**, *18*, 237–250. [CrossRef]
91. Estes, B.L.; Knapp, E.E.; Skinner, C.N.; Miller, J.D.; Preisler, H.K. Factors influencing fire severity under moderate burning conditions in the Klamath Mountains, northern California, USA. *Ecosphere* **2017**, *8*, e01794. [CrossRef]
92. Catry, F.X.; Rego, F.C.; Bação, F.L.; Moreira, F. Modeling and mapping wildfire ignition risk in Portugal. *Int. J. Wildl. Fire* **2009**, *18*, 921–931. [CrossRef]
93. Peris-Llopis, M.; González-Olabarria, J.R.; Mola-Yudego, B. Size dependency of variables influencing fire occurrence in Mediterranean forests of Eastern Spain. *Eur. J. For. Res.* **2020**, *139*, 525–537. [CrossRef]
94. Ricotta, C.; Bajocco, S.; Guglietta, D.; Conedera, M. Assessing the Influence of Roads on Fire Ignition: Does Land Cover Matter? *Fire* **2018**, *1*, 24. [CrossRef]
95. Romero-Calcerrada, R.; Novillo, C.J.; Millington, J.D.A.; Gomez-Jimenez, I. GIS analysis of spatial patterns of human-caused wildfire ignition risk in the SW of Madrid (Central Spain). *Landsc. Ecol.* **2008**, *23*, 341–354. [CrossRef]
96. Syphard, A.D.; Radeloff, V.C.; Keuler, N.S.; Taylor, R.S.; Hawbaker, T.J.; Stewart, S.I.; Clayton, M.K. Predicting spatial patterns of fire on a southern California landscape. *Int. J. Wildl. Fire* **2008**, *17*, 602–613. [CrossRef]
97. Ascoli, D.; Vacchiano, G.; Scarpa, C.; Arca, B.; Barbati, A.; Battipaglia, G.; Elia, M.; Esposito, A.; Garfì, V.; Lovreglio, R.; et al. Harmonized dataset of surface fuels under Alpine, temperate and Mediterranean conditions in Italy. A synthesis supporting fire management. *iForest* **2020**, *13*, 513–522. [CrossRef]
98. Lydersen, J.M.; Collins, B.M.; Brooks, M.L.; Matchett, J.R.; Shive, K.L.; Povak, N.A.; Kane, V.R.; Smith, D.F. Evidence of fuels management and fire weather influencing fire severity in an extreme fire event. *Ecol. Appl.* **2017**, *27*, 2013–2030. [CrossRef]
99. Stephens, S.L.; McIver, J.D.; Boerner, R.E.J.; Fettig, C.J.; Fontaine, J.B.; Hartsough, B.R.; Kennedy, P.L.; Schwilk, D.W. The effects of forest fuel-reduction treatments in the United States. *Bioscience* **2012**, *62*, 549–560. [CrossRef]
100. Abatzoglou, J.T.; Williams, A.P.; Barbero, R. Global Emergence of Anthropogenic Climate Change in Fire Weather Indices. *Geophys. Res. Lett.* **2019**, *46*, 326–336. [CrossRef]
101. Chappaz, F.; Ganteaume, A. Role of land-cover and WUI types on spatio-temporal dynamics of fires in the French Mediterranean area. *Risk Anal.* **2022**, 1–26. [CrossRef]